Fluctuations in nanoscale magnetoelectronics devices

Yabin Fan,[a] Igor V. Ovchinnikov, Wanjun Jiang, Robert N. Schwartz, and Kang L. Wang
Department of Electrical Engineering, University of California at Los Angeles, Los Angeles, California 90095, USA

(Received 13 July 2012; accepted 25 September 2012; published online 1 November 2012)

We analyze the quantum and thermal fluctuations in a magnetic nanoparticle that can be used as a component in magnetoelectronic devices and compare their influences on the basic modes of device operation at the nanoscale level. Within the framework of the effective Landau free energy constructed using a spin density functional approximation, we study the interplay between quantum and thermal fluctuations in different quantum numbers as the temperature and dimension of the particle are varied. Both theoretical and simulation results are presented for quantifying the quantum and thermal fluctuations. While quantum fluctuations hamper further miniaturization of today's electronic devices, our results suggest that the dominant factors affecting magnetoelectronic nanoscale devices are thermal fluctuations. © *2012 American Institute of Physics*. [http://dx.doi.org/10.1063/1.4759251]

I. INTRODUCTION

To continue scaling the feature size of semiconductor devices, there are two major issues: power dissipation and variability[1] as identified by the International Technology Roadmap for Semiconductors (ITRS).[2] The variability resides in the fact that there are both quantum and thermal fluctuations in the devices: quantum fluctuations due to the quantized/discrete values of state variables at the nanoscale level and thermal fluctuations ascribed to the statistical nature of state variables at finite temperature. For today's electronic devices, miniaturization has reached a point where variability of the threshold voltages of nanotransistors due to quantum fluctuations is significant even at room temperature. Magnetoelectronics[3] or spintronics, which utilizes the spin degrees of freedom of electrons, has emerged as a potential candidate in search of low power dissipation and low variability devices. In light of this, a natural question that arises is how fluctuations will affect the operation of magnetoelectronic devices and if there are any advantages, or possible drawbacks, in switching from the charge degrees of freedom in electronics to the spin in magnetoelectronics from the point of view of variability.

For typical magnetoelectronic devices, the system for which the variability is under consideration is the elemental nanoscale magnetic gate or the magnetic nanoparticle capacitively coupled to an electrode or a lead. Magnetic nanoparticles, e.g., Co nanoparticles[4,5] and the single-molecule magnets Mn_{12} and Fe_8,[6–9] have recently been theoretically studied mostly from the point of view of electron tunneling spectroscopy[10–15] or the spin-Berry phase associated with the tunneling.[16,17] Previously, we have analyzed the variability of electronic and spintronic nanoscale devices within the framework of a minimal ferromagnetic Hamiltonian[18] that was constructed by including different interactions. We studied both the quantum and thermal fluctuations in the total number of electrons, the total spin, and the projection of the spin vector on the easy axis within a magnetic nanoparticle. Here, in this paper, we consider in more detail the quantum and thermal fluctuations in a magnetic nanoparticle within the framework of the effective Landau free energy in a general open system under different gate voltages and magnetic fields. Moreover, we study and simulate more realistic nanoparticle device structures and reveal the interplay between quantum and thermal fluctuations in the different quantum numbers of the magnetic nanoparticle.

II. THEORETICAL MODEL

In physical terms, the magnetic nanoparticle in a magnetoelectronic circuit is an open many-body electron system exchanging, in addition to heat quanta, spins (or electrons) with the remaining parts of the circuit. Among the complete set of quantum numbers of this system are: the total number of electrons, $N = N_\uparrow + N_\downarrow$, where $N_{\uparrow,\downarrow}$ are the numbers of electrons in the spin-up and spin-down states, respectively; the total spin, $S = (N_\uparrow - N_\downarrow)/2$; and the projection of the total spin vector on the easy axis $\hat{z}$, S_z, which enumerates the spin multiplet levels, $S_z = S, S-1, \ldots, -S$. The thermodynamics of such a system is governed by the Landau free energy (or Ω-potential), where $\Omega = -\beta^{-1}\ln\Xi(\beta; V_i)$ and $\Xi(\beta; V_i)$ is the grand partition function[19]

$$\Xi(\beta; V_i) = \sum_{N,S,S_z} e^{-\beta(E(N,S,S_z)-(\mu+V_g)N - g\mu_B BS)}, \qquad (1)$$

where β is the inverse temperature in energy units, $\beta = 11600/T(\text{eV})$, with T in Kelvins; g is the g-factor of the nanoparticle and μ_B is the Bohr magneton. The energy of the nanoparticle is composed of two parts: the nanoparticle's self-energy, $E(N, S, S_z)$, and the external potential energies in the form of conjugate pairs, $-V_g N - g\mu_B BS$. Here, V_g is the gate voltage imposed by the electrode on the nanoparticle, B is the external magnetic field acting on the scalar length of the total spin vector, and μ is the chemical potential. The Ω-potential determines the statistical values, $\langle R_i\rangle = -\partial\Omega/\partial V_i$, as well as the mean square fluctuations in the quantum numbers, $\langle (R_i - \langle R_i\rangle)^2\rangle = -\beta^{-1}\partial^2\Omega/\partial V_i{}^2$. Here, for convenience, we used the reduced vector of the quantum numbers, $R = (N, S)$, and the reduced vector of the external fields, $V = (V_g, g\mu_B B)$.

[a]Electronic address: yabin@ee.ucla.edu.

In the following, we first consider the zero temperature (ground state) Ω-potential associated with the quantum numbers N and S for a nickel magnetic nanoparticle. Within spin density functional theory, the ground state Ω-potential at given N and S is a functional of the spin densities, $\rho_{\uparrow,\downarrow}(\vec{x})$, where $\vec{x}$ is the spatial point vector within the nanoparticle. The conduction band electrons in 3*d* transition metals are itinerant, so consequently the electron spin densities can be assumed constant over the whole volume of the nanoparticle. The spin densities have the simple form: $\rho_{\uparrow,\downarrow} = N_{\uparrow,\downarrow}/\mathcal{N}_a$, where $\mathcal{N}_a$ is the number of atoms in the nanoparticle. The self-energy of the nanoparticle can be constructed by including the band kinetic energy, the exchange energy, and the interaction energy.[12–14] One then obtains the ground state Ω-potential, Ω_0, which is a function of $N_\uparrow$ and $N_\downarrow$ (or N and S):[27]

$$\Omega_0(N_\uparrow, N_\downarrow) = \left(\sum_{\uparrow,\downarrow}\sum_{i=1}^{N_{\uparrow,\downarrow}}\epsilon_i\right) - \frac{\mathcal{J}}{\mathcal{N}_a}S^2 + \frac{\varepsilon_{cb}}{2}(N - Z\mathcal{N}_a)^2 - (\mu + V_g)N - g\mu_B BS, \quad (2)$$

where ϵ_i are the kinetic energies of the levels of spatial quantization, $\mathcal{J}$ is the exchange energy per atom, ε_{cb} is the Coulomb blockade energy, $\varepsilon_{cb} = e^2/\mathcal{C}$, with $\mathcal{C}$ being the capacitance of the nanoparticle, and Z is the number of conduction band electrons per atom ($Z = 10$ for nickel).

The kinetic energies ϵ_i of the spatial quantization of the nanoparticle can be found from the bulk density of states (DOS) of nickel, $\nu_{Ni}(\epsilon)$, which was evaluated using the Slater-Koster linear combination of atomic orbitals (SK-LCAO) method.[20] The DOS asymptotically approaches its bulk value for clusters $\mathcal{N}_a > 50$,[21] and in this limit, $\nu(\epsilon) \approx \mathcal{N}_a\nu_{Ni}(\epsilon)$. The average interlevel spacing is approximately $\delta\epsilon = 1/[\mathcal{N}_a\nu_{Ni}(\epsilon)]$ based on the assumption that the DOS of a nanoparticle is a set of δ-functions, each representing a quantum energy level, as shown in Fig. 1.

It is instructive to treat $N_\uparrow$ and $N_\downarrow$ as continuous variables, so that we can find the critical points of Ω_0 by solving the conditions, $\partial\Omega_0/\partial N_{\uparrow,\downarrow} = 0$, to obtain

$$\epsilon_{\uparrow,\downarrow} \mp \frac{\mathcal{J}S}{\mathcal{N}_a} + \varepsilon_{cb}(N - Z\mathcal{N}_a) - (\mu + V_g) \mp \frac{g\mu_B B}{2} = 0, \quad (3)$$

where $\epsilon_{\uparrow,\downarrow}$ are the Fermi energies for the spin-up and spin-down electrons, respectively. In the absence of the external fields ($V_g = 0$ and $B = 0$), the paramagnetic state, $N = Z\mathcal{N}_a, S = 0$ and $\epsilon_{\uparrow,\downarrow} = \mu$ fulfils the requirement. The second derivative with respect to S is: $\partial^2\Omega_0/\partial S^2 = 2(\nu_{Ni}(\mu)^{-1} - \mathcal{J})/\mathcal{N}_a$. If the right hand side of this equation is negative, the paramagnetic state is not stable and the system shifts to the ferromagnetic ground state, $S \neq 0$. The ferromagnetic ground state can be found from Eq. (3) by taking the difference $\Delta\epsilon = \epsilon_\uparrow - \epsilon_\downarrow = 2\mathcal{J}S/\mathcal{N}_a$. The Fermi energies can be found from the data in Fig. 1: $\epsilon_\uparrow = 9.02\text{eV}$ and $\epsilon_\downarrow = 7.93\text{eV}$. The number of spin-up and spin-down electrons, respectively, is:[20] $N_\uparrow = 5.33\mathcal{N}_a$, $N_\downarrow = 4.66\mathcal{N}_a$; thus, $2S/\mathcal{N}_a = (N_\uparrow - N_\downarrow)/\mathcal{N}_a = 0.66$. It, therefore, follows that $\mathcal{J} = \Delta\epsilon/0.66 = 1.6\text{eV}$ and hence the ferromagnetic state stability is consistent for nickel, since $\mathcal{J} > 1/\nu_{Ni}(\mu) \approx 0.49\text{eV}$, which is historically Stoner's criterion[22] for the ferromagnetism.

The solution to Eq. (3) gives two numbers, $\tilde{R} = (\tilde{N}, \tilde{S})$, which are functions of the external fields V_g and B. These numbers are not necessarily integers (or half-integers) for $\tilde{N}$ (or $\tilde{S}$). These numbers simply give the energetically preferred values of the minimized Ω-potential, and the actual ground state Ω-potential has the form, $\Omega_0 = \Omega_{\min} + (R_0 - \tilde{R})_i\,\mathcal{C}_{ij}^{-1}(R_0 - \tilde{R})_j/2$, where $R_0 = (N_0, S_0) = ([\tilde{N}], [2\tilde{S}]/2)$ is the ground state. Here, $[\tilde{N}]$ is the nearest integer to $\tilde{N}$ and $[2\tilde{S}]/2$ is the nearest half-integer to $\tilde{S}$; $\mathcal{C}_{ij}^{-1}$ is given by the second derivative (inverse capacitance) matrix, which is the sum of the kinetic and exchange part, $\mathcal{K}$, and the Coulomb part, $\mathcal{X}$; that is, $\mathcal{C}_{ij}^{-1} = \mathcal{K} + \mathcal{X}$, where

$$\mathcal{K} = \frac{1}{\mathcal{N}_a}\begin{bmatrix} \frac{\delta_\uparrow + \delta_\downarrow}{4} & \frac{\delta_\uparrow - \delta_\downarrow}{2} \\ \frac{\delta_\uparrow - \delta_\downarrow}{2} & \delta_\uparrow + \delta_\downarrow - 2\mathcal{J} \end{bmatrix}, \quad \mathcal{X} = \varepsilon_{cb}\begin{bmatrix} 1 & 0 \\ 0 & 0 \end{bmatrix}. \quad (4)$$

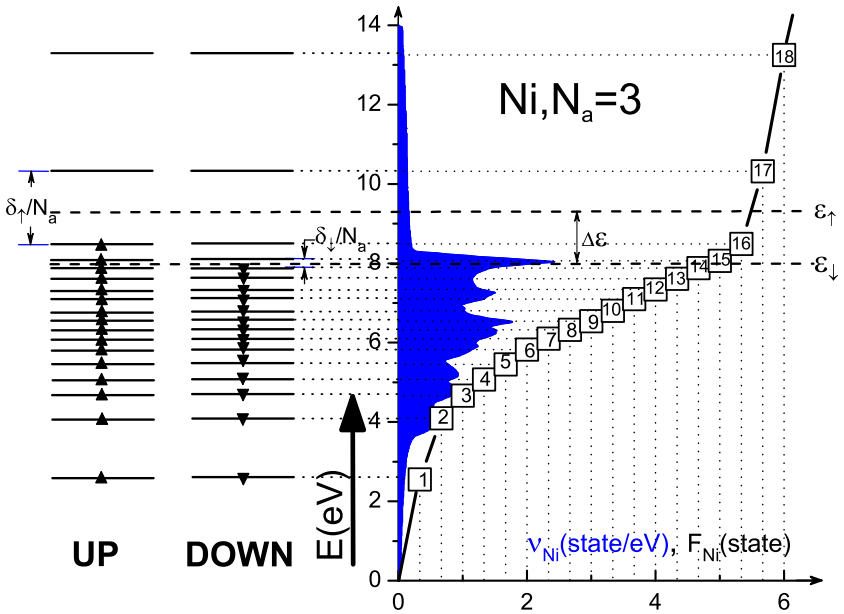

FIG. 1. The graphical representation of the energies of the spatial quantization levels in a nickel nanoparticle. The blue filled area ν_{Ni} represents the bulk DOS for either spin-up or spin-down electrons. The black curve F_{Ni} is the integrated DOS, and the numbered blocks indicate the positions of the quantized levels within a hypothetical $\mathcal{N}_a = 3$ nanoparticle. Shown on the left are the levels of the spin-up and spin-down electrons, respectively, as $N_{\uparrow,\downarrow} = 16, 14$. $\delta_{\uparrow,\downarrow}/\mathcal{N}_a = 5.42, 0.64\,\text{eV}/\mathcal{N}_a$ are the interlevel separations for the spin-up and spin-down electrons at their Fermi energies $\epsilon_{\uparrow,\downarrow}$. $\Delta\epsilon = \epsilon_\uparrow - \epsilon_\downarrow = 1\,\text{eV}$ is the exchange splitting.

Here, $\delta_{\uparrow,\downarrow} = \nu_{Ni}^{-1}(\epsilon_{\uparrow,\downarrow})$ are the normalized interlevel separations at the Fermi energies (for nickel $\delta_{\uparrow,\downarrow} = 5.42, 0.64$eV). This inverse capacitance matrix describes the coupling between the charge and spin quantum numbers, and is responsible for the observation of the variation in the total electron number N with external field B.[23]

At finite temperature, both quantum and thermal fluctuations need to be considered in the operation of a nanoparticle device. The Ω-potential at finite temperature is given as, $\Omega = \Omega_{\min} + \Theta(\beta; V_g, B)$, where the Θ-function is defined as

$$\Theta(\beta; V_g, B) = -\beta^{-1} \ln \sum_R e^{-\beta(R-\tilde{R})_i C_{ij}^{-1} (R-\tilde{R})_j/2}. \quad (5)$$

The Θ-function is periodic in both variables under the translations $\tilde{N} \to \tilde{N} + 1$ and $\tilde{S} \to \tilde{S} + 1/2$, and is a minimum at the quantized ground states (N_0, S_0). At low temperature ($\beta \to \infty$), Θ reduces down to the ground state form: $\Theta \simeq (R_0 - \tilde{R})_i C_{ij}^{-1} (R_0 - \tilde{R})_j/2$, and the statistical behavior is greatly suppressed. Obviously, different ground states are separated by the Coulomb blockade in the $\tilde{N}$ direction and by the kinetic and exchange blockade in the $\tilde{S}$ direction; see Fig. 2(a). These blockades become significant for small nanoparticles. The Ω-potential jumps among the quantized ground states through a tunneling mechanism.[13] By changing the magnetic and electric fields, the abrupt jumps among the ground states (N_0, S_0) give rise to the quantum fluctuations in these two quantum numbers; see Figs. 2(b) and 2(c).

As the temperature rises, the Θ-function can be viewed as a sum of identical 2-dimensional Gaussians centered at points on the $(\tilde{N}, \tilde{S})$-plane with integer (or half-integer) values for $\tilde{N}$(or $\tilde{S}$). These Gaussians are characterized by their magnitudes, $|\Delta N|$ and $|\Delta S|$, i.e., the thermal fluctuation magnitudes along the principal directions $\tilde{N}$ and $\tilde{S}$, where $|\Delta N| = \langle (N - \tilde{N})^2 \rangle^{1/2} = [T/(\varepsilon_{cb} + (\delta_\uparrow + \delta_\downarrow)/4\mathcal{N}_a)]^{1/2}$ and $|\Delta S| = \langle (S - \tilde{S})^2 \rangle^{1/2} = [T/(\delta_\uparrow + \delta_\downarrow - 2\mathcal{J})/\mathcal{N}_a]^{1/2}$, with the temperature, T, expressed in energy units. $|\Delta N|$ is shown in Fig. 2(d). When the temperature is increased, the individual Gaussians will effectively overlap with each other, as shown in Fig. 2(d), and eventually smear out the quantum fluctuations. Under these conditions, we obtain the classical linear response of the gate voltage V_g versus $\tilde{N}$, as well as the normal thermal noises (fluctuations). It is advisable to define the characteristic temperatures, T_N and T_S, which set the boundaries between the quantum and thermal fluctuations, as follows:

$$\langle (N - \tilde{N})^2 \rangle = \frac{T}{T_N}, \quad \langle (S - \tilde{S})^2 \rangle = \frac{T}{4T_S}, \quad (6)$$

where $T_N = \varepsilon_{cb} + (\delta_\uparrow + \delta_\downarrow)/4\mathcal{N}_a$ and $T_S = (\delta_\uparrow + \delta_\downarrow - 2\mathcal{J})/4\mathcal{N}_a$. The boundaries are defined by $|\Delta N| = 1$ and $|\Delta S| = 1/2$, which are equal to the intervals between the quantized ground states.

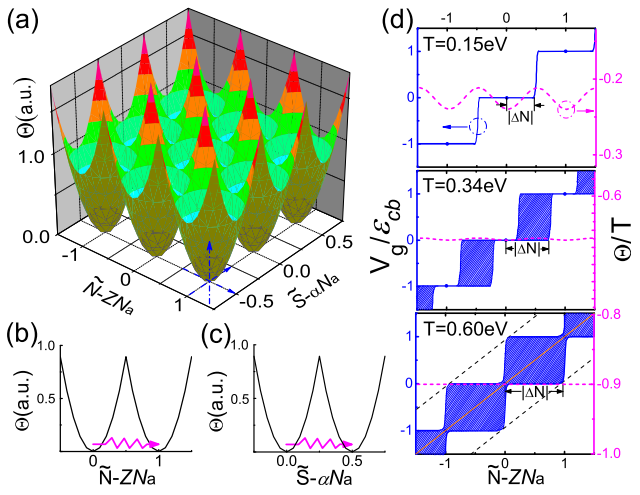

FIG. 2. (a) The Θ-function on the $(\tilde{N}, \tilde{S})$-plane of the ground state. Different quantized states are separated by the Coulomb blockade in the $\tilde{N}$ direction and by the kinetic and exchange blockade in the $\tilde{S}$ direction. [(b) and (c)] Schematics of the tunnelings along the $\tilde{N}$ and $\tilde{S}$ directions, respectively, which give rise to the quantum fluctuations. (d) From top to bottom, the figures show the evolution of the Θ-function (purple dashed) as the thermal energy increases. The Gaussians overlap with each other and finally smear out the quantum fluctuations. The V_g versus $\tilde{N}$ curve (blue solid) evolves from a stair-like to a linear function. $|\Delta N|$ is the magnitude of thermal fluctuations along the $\tilde{N}$ axis. $|\Delta N| = 0.5, 0.75, 1$ for thermal energy $T = 0.15$, 0.34, and 0.60 eV in a $\mathcal{N}_a = 100$ nickel nanoparticle.

III. SIMULATIONS AND RESULTS

In order to evaluate the Coulomb blockade energy ε_{cb}, we consider two models for the nanoparticles. The first model is a 3-dimensional (3D) spherical nanoparticle surrounded by uniform dielectric, e.g., SiO_2, where the capacitance is given by, $\mathcal{C}_{3D} = 4\pi k r$, with k being the dielectric constant of the silicon dioxide and $r = (3\mathcal{N}_a a^3/16\pi)^{1/3}$ being the radius of the nanoparticle; here, a is the lattice constant ($a = 0.35$ nm in nickel). The Coulomb blockade energy for the 3D spherical nanoparticle is $\varepsilon_{3D} = \frac{2.7}{\mathcal{N}_a^{1/3}}$(eV). The second model considered is a 2-dimensional (2D) planar nanoparticle that is isolated from the substrate by a high-k dielectric, e.g., HfO_2. The capacitance of the 2D planar nanoparticle is given as $\mathcal{C}_{2D} = k\pi r^2/d$, where r is the radius of the planar nanoparticle and d is the thickness of the dielectric. For the 2D configuration, the Coulomb blockade energy is $\varepsilon_{2D} = \frac{67.4}{\mathcal{N}_a}$(eV) when the thicknesses of the planar nanoparticle and the dielectric are both one nanometer. These two models set the range of Coulomb blockade energy for a more realistic nano-gate in a transistor and are compared with the computer simulation technology particle studio (CST-PS) simulations.[25]

The CST-PS, which solves Maxwell's equations based on the finite integration method, is a specialist tool for the fast and accurate 3D analysis of charged particle dynamics in 3D electromagnetic fields. In the CST-PS simulations, we use two different configurations to simulate the above two models, as shown in Figs. 3(a) and 3(b), respectively. In Fig. 3(a), the central sphere represents a 3D spherical nickel nanoparticle that is surrounded by uniform dielectric SiO_2 located in the region between radius r_1 and r_2; the outer shell between radius r_2 and r_3 represents the boundary that is grounded to zero voltage; we set $r_2 = 115$ nm and $r_3 = 120$ nm in the simulation. In Fig. 3(b), the central part represents a 2D planar nickel nanoparticle with radius r_1; the layer behind the nanoparticle is the dielectric HfO_2 with radius r_2; the layer behind HfO_2 represents the conducting channel with radius r_3 that exists in currently used integrated circuit chips and is

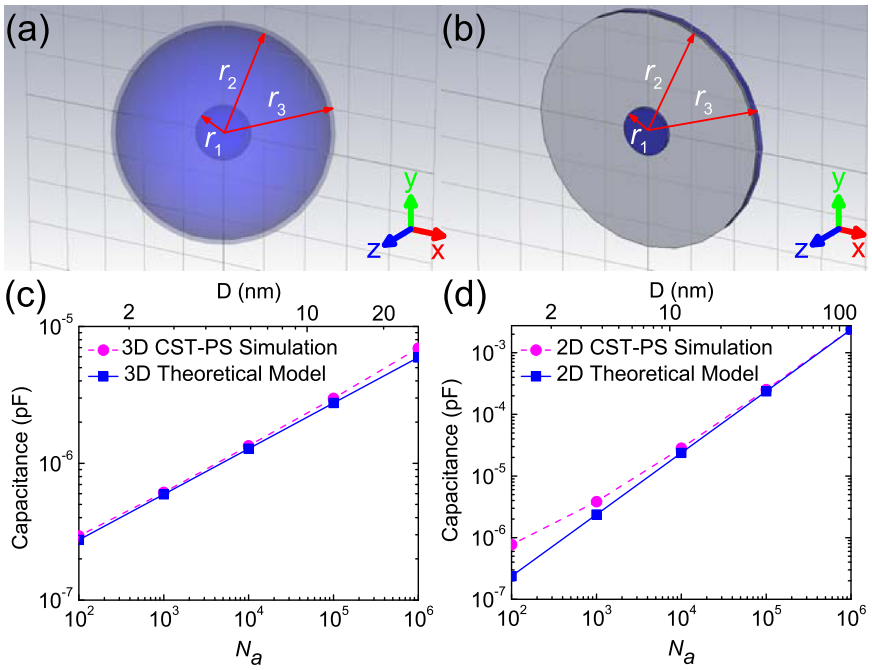

FIG. 3. (a) The 3D spherical nanoparticle in the computer simulation technology particle studio (CST-PS) software interface. r_1 is the radius of the nickel nanoparticle; the region between radius r_1 and r_2 is the dielectric SiO_2; the outer shell between radius r_2 and r_3 represents the boundary that is grounded to zero voltage; $r_2 = 115$ nm and $r_3 = 120$ nm. (b) The 2D planar nanoparticle in the CST-PS software interface. r_1 is the radius of the planar nickel nanoparticle disk; the layer behind the nanoparticle is the dielectric HfO_2 with radius r_2; the layer behind HfO_2 represents the conducting channel with radius r_3 in the substrate and is grounded to zero voltage; the thicknesses of the planar nanoparticle and the HfO_2 layer are both one nanometer; $r_2 = r_3 = 50$ nm. (c) The 3D spherical nickel nanoparticle capacitance obtained from the simulation and the theoretical model, respectively, as a function of the number of atoms $\mathcal{N}_a$ (bottom axis) and the diameter of the particle (top axis). (d) The 2D planar nickel nanoparticle capacitance obtained from the simulation and the theoretical model, respectively, as a function of the number of atoms $\mathcal{N}_a$ (bottom axis) and the diameter of the particle (top axis).

grounded to zero voltage; the thicknesses of the planar nanoparticle and the HfO_2 layer are both set to be one nanometer; we also set $r_2 = r_3 = 50$ nm in the simulation. At a given voltage imposed on the nanoparticle, the CST-PS software calculates the charge distributions on the nanoparticle and hence, the capacitance is obtained; the results are plotted in Figs. 3(c) and 3(d) for the 3D and 2D configurations, respectively. The predictions from the above two theoretical models are also plotted and they agree nicely with the simulation results. The small deviation between the 2D configuration theoretical model and the simulation in the small nanoparticle limit is mainly due to the fact that the 2D planar nanoparticle geometrically approaches a 3D spherical nanoparticle at small scale. The Coulomb blockade energies ($\varepsilon_{cb} = e^2/\mathcal{C}$) obtained from the two configurations are plotted in the inset of Fig. 4.

The characteristic temperatures (in eV units) T_N of the above two theoretical models are, $T_{3D} = \frac{2.7}{\mathcal{N}_a^{1/3}}$ and $T_{2D} = \frac{69}{\mathcal{N}_a}$, respectively, while the characteristic temperature T_S is, $T_S = \frac{0.7}{\mathcal{N}_a}$, according to Eq. (6). If the device is required to operate at room temperature, $T_0 = 26$ meV, then the size of the nanoparticle will be limited such that the number of atoms in the nanostructures are $(\mathcal{N}_a)_{3D} = 1.1 \times 10^6$ and $(\mathcal{N}_a)_{2D} = 2.7 \times 10^3$ in order for the electrons' number fluctuation to achieve the quantum limit in the 3D and 2D models, respectively; whereas $(\mathcal{N}_a)_S = 30$ is required for the total spin fluctuation to be quantized.

IV. SPIN ANISOTROPY

It is unlikely, however, that the quantum number S can be employed in information processing. In fact, in magnetoelectronics, the information is supposed to be encoded in the spin vector projection S_z, just as it is used for storing information in magnetic memory devices.[24] The only measurable quantum number is S_z; however, the quantum number S sets the range of fluctuation for S_z, given that $|S_z| \leq S$.

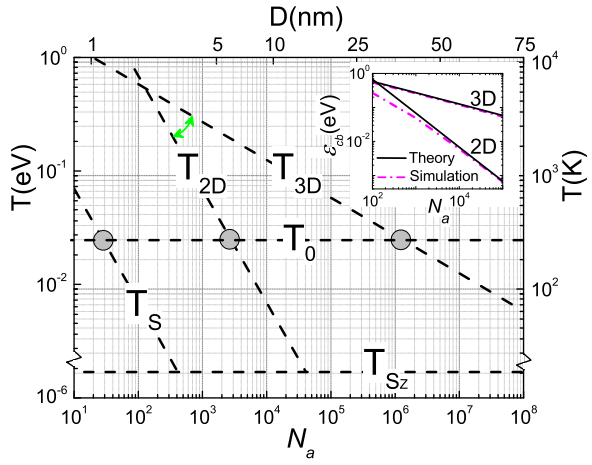

FIG. 4. Domains of fluctuations for the three quantum numbers N, S, and S_z. T_{2D} and T_{3D} give the range for T_N. The lines T_{2D}, T_{3D}, T_S, and T_{S_z} separate the areas of quantum (to the left and below) and thermal (to the right and above) fluctuations of the corresponding quantum numbers. At room temperature, $T_0 = 26$ meV and therefore the fluctuation in the quantum number S gives the limiting number of 30 atoms versus the electronics counterpart of $10^3 \sim 10^6$ atoms. T_{S_z} is far below T_0, which means S_z is less affected by the quantum fluctuations at room temperature. Inset: The comparisons between the theoretical models and the CST-PS simulations of the Coulomb blockades in the 2D and 3D configurations, respectively.

The additional term in the Ω-potential associated with the quantum number S_z is due to the spin anisotropy energy,

$$\Delta\Omega(S, S_z) = \frac{\varepsilon_{ae}}{2\mathcal{N}_a}\left\langle \hat{S}_x^2 + \hat{S}_y^2 \right\rangle = \frac{\varepsilon_{ae}}{2\mathcal{N}_a}\left[S(S+1) - S_z^2\right], \quad (7)$$

where ε_{ae} is the spin anisotropy energy per atom. The spin anisotropy energy arises from the magnetocrystalline anisotropy or shape anisotropy within the nanoparticle. In the ground state $|S_z = S\rangle$, $\Delta\Omega$ can be approximately given in the harmonic oscillator form, $\Delta\Omega \approx \alpha\varepsilon_{ae}\hat{c}^\dagger\hat{c}$, where α is the bulk value of the magnetization per atom (for nickel $\alpha = 0.33$), $\hat{c} = (\hat{S}_x - i\hat{S}_y)/(\sqrt{2S})$, and $[\hat{c}^\dagger, \hat{c}] = 1$, are the creation and annihilation operators within the spin multiplet Fock space. The levels are equally separated on the energy scale, and the interlevel separation gives the S_z characteristic temperature $T_{S_z} = \alpha\varepsilon_{ae}$. For $3d$ transition metals, which are soft ferromagnets, the magnitude of ε_{ae} is of the order of several dozens of μeV (for nickel $\varepsilon_{ae} \approx 12\,\mu$eV).[26] The quantum fluctuation in S_z can be seen at extremely low temperature, e.g., the effect of the magnon-electron coupling on the low-temperature electron conductance was recently studied in Ref. 10. The fluctuation in S_z, i.e., the reorientation of the spin vector, takes the place of the long-wavelength spin waves in the Goldstone mode.

V. CONCLUSIONS

In summary, we have constructed the effective Landau free energy of a magnetic nanoparticle and studied the interplay between the quantum and thermal fluctuations in different quantum numbers. Both the theoretical analysis and simulations are carried out in order to quantify the quantum and thermal fluctuations. Quantum versus thermal fluctuations are summarized in Fig. 4. The lines separating the quantum and thermal fluctuations are drawn in the temperature-size plane for the three quantum numbers—the number of electrons N, the total spin S, and the projection of the spin vector on the easy axis S_z. In practice, it is S_z that is used in magnetoelectronics. Since T_{S_z} is far below the room temperature T_0, it can be concluded that magnetoelectronic devices will be limited only by thermal fluctuations and not by quantum fluctuations, which hamper the further miniaturization of today's electronic devices at room temperature.

ACKNOWLEDGMENTS

This work was supported by the Focus Center on Functional Engineered NanoArchitectonics (FENA) and the Western Institute of Nanoelectronics (WIN) at UCLA.

[1]G. E. Moore, Electronics **38**, 114 (1965).
[2]See http://www.itrs.net/ for ITRS news: More than Moore White Paper.
[3]S. A. Wolf, D. D. Awschalom, R. A. Buhrman, J. M. Daughton, S. von Molnar, M. L. Roukes, A. Y. Chtchelkanova, and D. M. Treger, Science **294**, 1488 (2001), and references therein.
[4]S. Guëron, M. M. Deshmukh, E. B. Myers, and D. C. Ralph, Phys. Rev. Lett. **83**, 4148 (1999).
[5]M. M. Deshmukh, S. Kleff, S. Guëron, E. Bonet, A. N. Pasupathy, J. von Delft, and D. C. Ralph, Phys. Rev. Lett. **87**, 226801 (2001).
[6]C. Paulsen, J. G. Park, B. Barbara, R. Sessoli, and A. Caneschi, J. Magn. Magn. Mater. **140**, 379 (1995); J. R. Friedman, M. P. Sarachik, J. Tejada, and R. Ziolo, Phys. Rev. Lett. **76**, 3830 (1996); L. Thomas, F. Lionti, R. Ballou, D. Gatteschi, R. Sessoli, and B. Barbara, Nature (London) **383**, 145 (1996).
[7]E. del Barco, A. D. Kent, S. Hill, J. M. North, N. S. Dalal, E. M. Rumberger, D. N. Hendrickson, N. Chakov, and G. Christou, J. Low Temp. Phys. **140**, 119–174 (2005).
[8]C. Sangregorio, T. Ohm, C. Paulsen, R. Sessoli, and D. Gatteschi, Phys. Rev. Lett. **78**, 4645–4648 (1997).
[9]W. Wernsdorfer and R. Sessoli, Science **284**, 133 (1999).
[10]L. Michalak, C. M. Canali, and V. G. Benza, Phys. Rev. Lett. **97**, 096804 (2006).
[11]S. Kleff, J. von Delft, M. M. Deshmukh, and D. C. Ralph, Phys. Rev. B **64**, 220401 (2001).
[12]S. Kleff and J. von Delft, Phys. Rev. B **65**, 214421 (2002).
[13]C. M. Canali and A. H. MacDonald, Phys. Rev. Lett. **85**, 5623 (2000).
[14]A. Cehovin, C. M. Canali, and A. H. MacDonald, Phys. Rev. B **68**, 014423 (2003).
[15]G. Usaj and H. U. Baranger, Europhys. Lett. **72**, 110 (2005).
[16]G. González and M. N. Leuenberger, Phys. Rev. Lett. **98**, 256804 (2007).
[17]W. Wernsdorfer, A. Caneschi, R. Sessoli, D. Gatteschi, A. Cornia, V. Villar, and C. Paulsen, Europhys. Lett. **50**, 552 (2000).
[18]I. V. Ovchinnikov and K. L. Wang, Appl. Phys. Lett. **92**, 093503 (2008).
[19]D. L. Goodstein, *States of Matter* (Prentice Hall, New Jersey, 1975), pp. 19–49.
[20]D. A. Papaconstantopoulos, *Handbook of the Band Structure of Elemental Solids* (Plenum, New York, 1986).
[21]I. M. L. Billas, A. Chtelain, and W. A. de Heer, Science **265**, 1682 (1994).
[22]E. C. Stoner, Proc. R. Soc. London, Ser. A **165**, 372 (1938).
[23]K. Ono, H. Shimada, and Y. Ootuka, J. Phys. Soc. Jpn. **66**, 1261 (1997); **67**, 2852 (1998).
[24]E. M. Chudnovsky and L. Gunther, Phys. Rev. Lett. **60**, 661 (1988); J. Tejada, E. M. Chudnovsky, E. del Barco, J. M. Hernandez, and T. P. Spiller, Nanotechnology **12**, 181–186 (2001); M. N. Leuenberger and D. Loss, Nature (London) **410**, 789 (2001).
[25]Computer Simulation Technology Particle Studio online help, (2012).
[26]J. Stöhr and H. C. Siegmann, *Magnetism from Fundamentals to Nanoscale Dynamics* (Springer, *New York*, 2006).
[27]Throughout the paper, we use the two pairs $N_\uparrow, N_\downarrow$ and N, S interchangeably.